

Ordered magnetic state in PrFe₄Sb₁₂ single crystals

N. P. Butch, W. M. Yuhasz, P.-C. Ho, J. R. Jeffries, N. A. Frederick, T. A. Sayles, X. G. Zheng,* and M. B. Maple
*Department of Physics and Institute for Pure and Applied Physical Sciences, University of California,
 San Diego, La Jolla, California 92093, USA*

J. B. Betts and A. H. Lacerda
National High Magnetic Field Laboratory/Los Alamos National Laboratory, Los Alamos, New Mexico 87545, USA

F. M. Woodward and J. W. Lynn
NIST Center for Neutron Research, National Institute of Standards and Technology, Gaithersburg, Maryland 20899-8562, USA

P. Rogl
Institut für Physikalische Chemie, Universität Wien, A-1090 Wien, Währingerstrasse 42, Austria

G. Giester
Institut für Mineralogie und Kristallographie, Universität Wien, A-1090 Wien, Althanstrasse 14, Austria
 (Received 10 November 2004; revised manuscript received 27 January 2005; published 22 June 2005)

The filled skutterudite compound Pr_{0.87}Fe₄Sb₁₂ was prepared in single-crystal form and characterized via x-ray-diffraction, neutron-diffraction, specific-heat, electrical-resistivity, and magnetization measurements. Long-range magnetic ordering occurs at $T_c \approx 4.1$ K, with the bulk magnetization described by the critical exponents $\beta=0.57$, $\gamma=0.884$, and $\delta=2.55$. The magnetic structure consists of ordered moments on both Pr and Fe sites and may involve a ferrimagnetic arrangement. The electrical resistivity exhibits a very weak dependence on both applied magnetic field and pressure at most temperatures, but at low temperatures, its power-law temperature-dependence varies with magnetic field. Specific-heat measurements indicate an enhanced effective mass.

DOI: 10.1103/PhysRevB.71.214417

PACS number(s): 75.40.Cx, 71.27.+a, 71.70.Ch

I. INTRODUCTION

Ternary skutterudite compounds RT_4X_{12} , with R =alkali, alkaline earth, lanthanide, or actinide; T =Fe, Ru, or Os; and X =P, As or Sb, have composed a fertile area of research over the past several years. These compounds exhibit a rich variety of correlated-electron phenomena, including valence fluctuations in YbFe₄Sb₁₂,¹ ferromagnetism in SmFe₄P₁₂,² and NdOs₄Sb₁₂,³ Kondo insulating behavior in CeOs₄Sb₁₂,⁴ and superconductivity in LaFe₄P₁₂.⁵ The compounds crystallize in a cubic structure with the $Im\bar{3}$ space group.⁶ Each T atom is surrounded by an octahedron of X atoms, slightly canted with respect to the cubic axes, while the R atoms occupy bcc sites, filling the interstices between the octahedra.

Pr-based filled skutterudites, in particular, have demonstrated an unusual variety of ordered ground states. The compound PrRu₄P₁₂ undergoes a metal-insulator transition at ~ 60 K,^{7,8} while PrRu₄Sb₁₂ displays superconductivity at temperatures less than 1.3 K,⁹⁻¹¹ and PrRu₄As₁₂ has a superconducting transition at 2.4 K.¹² The compound PrOs₄P₁₂ exhibits metallic paramagnetism over the whole temperature range that has been measured,⁷ whereas PrOs₄Sb₁₂ is a heavy-fermion superconductor with a transition temperature of 1.85 K, in which the unusual superconductivity is possibly mediated by electric quadrupole fluctuations.^{13,14} Evidence of quadrupolar ordering is also present in the PrFe₄P₁₂ system.¹⁵⁻¹⁷ In addition, studies of chemical substitution into

the Pr-based filled skutterudites are yielding interesting results.^{18,19}

The compound PrFe₄Sb₁₂ is the only Pr-based filled skutterudite that unambiguously shows magnetic ordering. The first published magnetization measurements reported unusual field dependence: a small, unsaturated magnetic moment in an applied magnetic field of 5.5 T, at about half of the Pr³⁺ free-ion value, and small coercivity and remanence.²⁰ Measurements of specific heat in field indicated a large low temperature electronic contribution along with non-Fermi-liquid behavior that was induced by applied magnetic fields ~ 3 T. Non-Fermi-liquid behavior was observed in the electrical resistivity at the same fields and Fermi-liquid behavior was recovered at higher fields.²¹ A subsequent study of crystalline electric field effects assigned a magnetic Γ_5 ground state to Pr³⁺, based on magnetization, resistivity, and specific heat data. It was further determined that the Fe-Sb sublattice also carries a magnetic moment, although the nature of the magnetic order could not be identified.²²

In order to elucidate the nature of the magnetic ordering in PrFe₄Sb₁₂, measurements of specific heat, magnetization, and electrical resistivity have been performed on single crystals of Pr_{0.87}Fe₄Sb₁₂. Magnetization measurements demonstrate long-range magnetic ordering with a transition at ~ 4.1 K, via scaling and modified Arrott analysis, both ac and dc susceptibility, and neutron diffraction. This is corroborated by low-temperature specific-heat data, which display a broad peak centered at ~ 4 K and also indicate an enhanced quasiparticle effective mass. Measurements of

TABLE I. $\text{Pr}_{0.87}\text{Fe}_4\text{Sb}_{12}$ single-crystal structural data determined at $T=296$ K. The crystal structure is $\text{LaFe}_4\text{P}_{12}$ type with space group $\text{Im}\bar{3}$ (No. 204).

$\text{PrFe}_4\text{Sb}_{12}$					
Crystal size	$54 \times 54 \times 81 \mu\text{m}^3$	Lattice parameter a [\AA]	9.140(1)	Density ρ [g/cm^3]	7.939
Reflections in refinement	$436 \leq 4\sigma(F_0)$ of 463	Number of variables	12	2θ Range	$2^\circ < 2\theta < 80^\circ$
Goodness of fit	1.176	$R_F^2 = \sum F_0^2 - F_c^2 / \sum F_0^2$	0.0172		
Pr in $2a$ (0, 0, 0)		Pr: $U_{11}=U_{22}=U_{33}$	0.0201(2)	Interatomic distances [\AA]	
Occupancy	0.871(5)	[\AA^2]		Pr - 12 Sb	3.4027
Fe in $8c$ (1/4, 1/4, 1/4);		Fe: $U_{11}=U_{22}=U_{33}$	0.0051(1)	Interatomic distances [\AA]	
Occupancy	1.00(1)	[\AA^2]		Fe - 6 Sb	2.5522
Sb in $24g$ (0, y , z); y :	0.16021(2)	Sb: U_{11}	0.0050(1)	Interatomic distances [\AA]	
z :	0.33604(2)	U_{22} [\AA^2]	0.0069(1)	Sb - 1 Sb	2.9972
Occupancy	1.00(1)	U_{33}	0.0089(1)	- 1 Sb	2.9287
				- 2 Fe	2.5522
				- 1 Pr	3.4027

electrical resistivity indicate very little magnetic field and pressure dependence.

II. EXPERIMENT

Single crystals of $\text{Pr}_{0.87}\text{Fe}_4\text{Sb}_{12}$ were grown by a self-flux method in excess molten Sb. Elemental Pr (3N), Fe (3N), and Sb (6N) were combined in the atomic ratio 1:4:20 and prepared as described in a previous article.¹⁸ The crystals were generally cubic in shape, and tended to grow in clusters. Dimensions of most crystals were less than 1 mm.

Crystal quality was determined by x-ray diffractometry. To assess bulk impurity content, several single crystals were ground and powder x-ray diffraction was performed with a Rigaku D/MAX B. X-ray structural refinement was carried out at the Universität Wien. After preliminary inspection with an AXS-Gadds texture goniometer, precision x-ray measurements of several trimmed single crystals were performed in transmission on a four-circle Nonius Kappa diffractometer equipped with a CCD area detector, using graphite-monochromated $\text{Mo-K}\alpha$ radiation ($\lambda=0.071073$ nm). Orientation matrix and unit cell parameters were derived using the program DENZO.²³ Absorption corrections were not necessary because of the regular crystal shape and small dimensions.

Specific heat $C_p(T)$ measurements, over the temperature T range $0.6 \text{ K} \leq T \leq 82 \text{ K}$, were performed on a ^3He refrigerator-based semi adiabatic calorimeter. Because of their small individual size, a number of single crystals, with a total mass of 49.9 mg, were measured together.

For $2 \text{ K} \leq T \leq 300 \text{ K}$ and applied magnetic fields H up to 9 T, electrical resistivity $\rho(H, T)$ measurements were performed in a Quantum Design Physical Properties Measurement System (PPMS). For $T \leq 2.6 \text{ K}$, $\rho(H, T)$ was measured in ^3He - ^4He dilution refrigerators at UCSD ($H \leq 8 \text{ T}$) and at the National High Magnetic Field Laboratory at Los Alamos

National Laboratory ($8 \text{ T} \leq H \leq 18 \text{ T}$). Resistivity was measured at constant currents of 100 and 300 μA , with magnetic fields applied perpendicular to the current flow. Resistivity under applied pressure P was measured in a quasihydrostatic Be-Cu cell over the range $1 \text{ atm} \leq P \leq 22.9 \text{ kbar}$ and the temperature range $1.2 \text{ K} \leq T \leq 300 \text{ K}$ in a ^4He cryostat, with applied current of 1-10 mA, using an ac resistance bridge. Pressure was determined from inductive measurement of the superconducting transition of a Pb manometer.

Magnetization $M(H, T)$ measurements were performed in Quantum Design SQUID magnetometers for $1.8 \text{ K} \leq T \leq 300 \text{ K}$ in H up to 5.5 T. AC magnetic susceptibility $\chi_{ac}(T)$ was used to screen crystals for a sharp magnetic transition. Measurement of $M(H, T)$ in a constant H was subsequently performed, with H parallel to [001].

The magnetic structure of two $\text{Pr}_{0.87}\text{Fe}_4\text{Sb}_{12}$ single crystals was investigated by neutron diffraction at the NIST Center for Neutron Research on the thermal triple axis instrument BT-7 in two-axis mode with $E_i=13.4075 \text{ meV}$ (2.47 \AA), and on the thermal triple axis spectrometer BT-9 in two-axis mode with $E_i=50 \text{ meV}$ (1.2791 \AA). The shorter wavelength was used in the second set of measurements to reduce extinction effects observed in the first measurement.

III. RESULTS

A. X-ray diffraction

X-ray powder-diffraction patterns indicated single phase $\text{PrFe}_4\text{Sb}_{12}$ as diffraction peaks due to impurities were not detected. For the single crystals, structures were refined using the program SHELXS-97.²⁴ Parameters determined from the single crystal x-ray analysis are listed in Table I. The crystals had a $\text{LaFe}_4\text{P}_{12}$ -type bcc structure,⁶ a lattice parameter $a=9.140 \text{ \AA}$ (unit cell volume of 763.6 \AA^3) and a Pr site occupancy of 0.87. The partial vacancy of the rare-earth site is not uncommon in the filled skutterudite compounds and

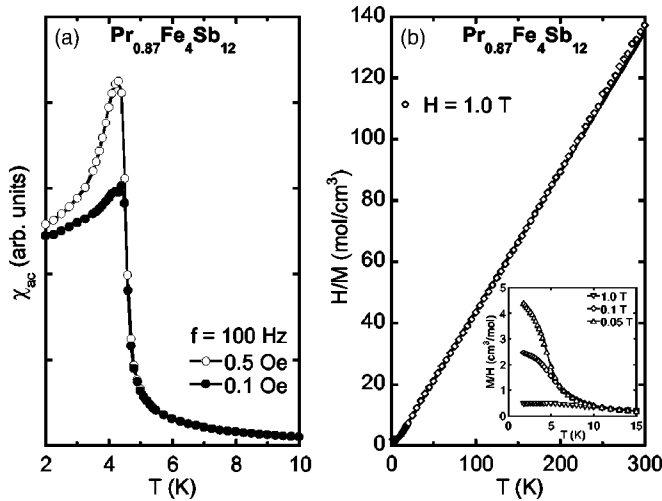


FIG. 1. (a) ac magnetic susceptibility $\chi_{ac}(T)$ at amplitudes of 0.5 (open) and 0.1 Oe (filled), indicating the onset of magnetic ordering between 4 and 5 K. (b) Inverse dc magnetic susceptibility H/M up to 300 K, indicating Curie-Weiss T -dependence. The inset shows low- T dc magnetic susceptibility M/H in various applied fields.

can vary between samples with the same nominal composition. Previous studies of polycrystalline $\text{PrFe}_4\text{Sb}_{12}$ reported Pr occupancy of 0.73,²¹ and later a lattice parameter $a=9.1369 \text{ \AA}$ and 3% Sb impurity content.²² Although sample properties should depend on rare-earth occupancy, comparable effects arise from differences in microstructure and phase homogeneity, which are also sample dependent. In order to simplify the following discussion, data from various samples are weighted equally and site occupancy is analyzed only when it can be plainly accounted for.

B. Bulk magnetization

A plot of $\chi_{ac}(T)$ of a $\text{Pr}_{0.87}\text{Fe}_4\text{Sb}_{12}$ single crystal is shown in Fig. 1(a). The temperature of the inflection point in $\chi_{ac}(T)$ is ~ 4.6 K, similar to results found for polycrystalline $\text{Pr}_{0.73}\text{Fe}_4\text{Sb}_{12}$,²² while the peak in $\chi_{ac}(T)$ occurs at ~ 4.2 K. The peak position and shape are independent of frequency, indicating the absence of spin glass behavior.

The same crystal was measured in constant applied magnetic field H , aligned with [001]. The T dependence of M in constant $H=1$ T is displayed in the plot of $\chi_{dc}^{-1}(T)$ in Fig. 1(b). In addition, the single crystal was rotated through [111] with no significant change in M , suggesting little magnetic anisotropy. The susceptibility is described well by a Curie-Weiss law down to approximately 20 K. The line is a fit to the data for $20 \text{ K} \leq T \leq 200 \text{ K}$, which indicates an effective moment $\mu_{\text{eff}}=4.34 \mu_B/\text{f.u.}$ In Fig. 2, a plot of $\chi_{dc}^{-1}(T)$ for $H=0.1$ T more clearly illustrates the linearity down to ~ 20 K. Also shown is a fit to the data from $20 \text{ K} \leq T \leq 40 \text{ K}$, which yields values of the Curie-Weiss temperature $\theta_{\text{CW}}=4.04$ K and effective moment $\mu_{\text{eff}}=4.13 \mu_B/\text{f.u.}$ The difference between the high- and low-temperature calculated moments may be due to crystalline electric field (CEF) effects, which are prominent in the rare earth filled skutterudites. The measured μ_{eff} exceeds the the-

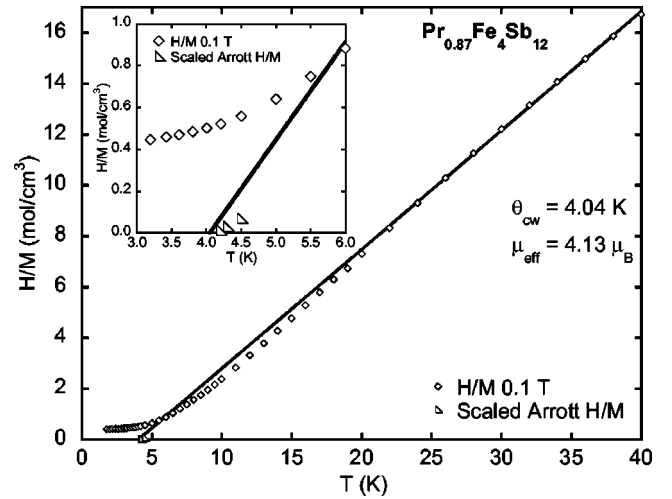


FIG. 2. Inverse dc magnetic susceptibility H/M at low T , showing deviation from Curie-Weiss behavior at ~ 20 K. The inset emphasizes the agreement between the Curie-Weiss fit and the scaled Arrott analysis discussed in the text.

oretical free ion Pr^{3+} moment of $3.58 \mu_B$ and is comparable to effective moment values found in studies of polycrystalline $\text{PrFe}_4\text{Sb}_{12}$ by Danebrock, Evers, and Jeitschko,²⁰ and Bauer and co-workers,^{21,22} who attributed the extra moment to a contribution from the Fe-Sb sublattice.

Isothermal magnetization $M(H)$ curves at several temperatures in the vicinity of the magnetic transition temperature T_c are shown in Fig. 3. It is immediately apparent that $M(H)$ does not saturate at the highest achieved $H=5.5$ T. In fact, $M(5.5 \text{ T}) \approx 1.65 \mu_B/\text{f.u.}$ is only approximately half of the theoretical free ion Pr^{3+} saturation moment $M_{\text{sat}}=gJ=3.2 \mu_B$. The coercivity is very low, with $H_{\text{crv}} \leq 1$ mT, and the remanent magnetization is less than $0.2 \mu_B/\text{f.u.}$ Another interesting feature of the M isotherms

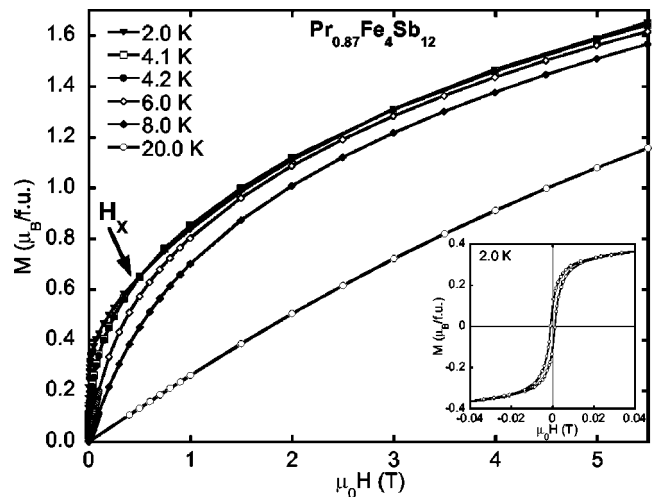


FIG. 3. Magnetization $M(H)$ isotherms for several temperatures above and below the magnetic ordering transition. Below 4.2 K, the $M(H)$ curves coalesce at an applied field $H_x \approx 0.5$ T. The inset shows a hysteresis loop at temperature $T=2$ K, demonstrating the small coercivity and remanence of $\text{Pr}_{0.87}\text{Fe}_4\text{Sb}_{12}$.

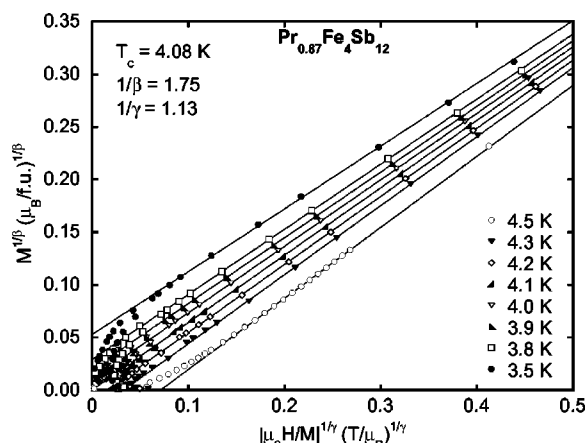


FIG. 4. Scaled Arrott plot demonstrating linear magnetization $M^{1/\beta}$ isotherms evenly spaced in temperature. The lines were fit to $M^{1/\beta}$ corresponding to intermediate values of the field H , as discussed in the text.

for $T < T_c$ is their apparent coalescence at $H_X \approx 0.5$ T.

In order to more clearly characterize the magnetic ordering evident in $\text{Pr}_{0.87}\text{Fe}_4\text{Sb}_{12}$, $M(H)$ isotherms were plotted on a modified Arrott plot (Fig. 4). On standard (mean-field) Arrott plots of M^2 vs H/M , the M^2 isotherms for $\text{Pr}_{0.87}\text{Fe}_4\text{Sb}_{12}$ display significant curvature for all H . In order to recover parallel, linear isotherms in the vicinity of the magnetic transition temperature T_c , it was necessary to invoke the Arrott-Noakes equation of state and accordingly plot $|M|^{1/\beta}$ vs $|H/M|^{1/\gamma}$.²⁵ To choose appropriate scaling exponents β and γ , an approximate $T_c \approx 4.1$ K was first determined along with the scaling exponent $\delta = 2.55$, from a plot of $\partial \ln H / \partial \ln M$ vs H . The three exponents are typically defined for reduced magnetization m , field h , and temperature $t = (T - T_c)/T_c$ by $m \sim t^\beta$, $m \sim h^{1/\delta}$, and $\partial m / \partial h = \chi \sim t^{-\gamma}$, and are related by $\delta - 1 = \gamma / \beta$. Analysis of the slopes of $M(H)$ isotherms for $T > T_c$ in the vicinity of $H = 0$ yielded an initial estimate of $\gamma = 1$, which set $\beta = 0.645$. Plotting scaled $H^* = H/|t|^{\delta\beta}$ vs scaled $M^* = |M|/|t|^\beta$ [Fig. 5(a)] collapsed the $M(H)$ data within the critical T range $3.5 \text{ K} \leq T \leq 4.5 \text{ K}$ onto two curves, corresponding to $T > T_c$ and $T < T_c$. A limited range of $M(H)$, $0.02 \text{ T} \leq H \leq 2 \text{ T}$, was used because this analysis is only applicable over mid range $M(H)$ due to the presence of magnetic domains at low H and to the effects of terms of higher order in M at higher H . Varying β , δ , and T_c to achieve the best fit resulted in values of $\beta = 0.57$, $\delta = 2.55$, and $T_c = 4.15$ K, setting $\gamma = 0.884$. It is evident from Fig. 4 that these critical exponents transform the M isotherms into parallel lines, evenly spaced in T , over the $M(H)$ range that was used in the scaling analysis. This linear T dependence is more clearly illustrated in a plot of the $M^{1/\beta}$ intercepts vs T [Fig. 5(b)]. A linear fit to these points indicates a magnetic ordering temperature $T_c = 4.08$ K, consistent with the $T_c = 4.15$ K that was determined from the scaling analysis [Fig. 5(a)]. The $M^{1/\beta}$ intercept of the linear fit, raised to the β power, has a value of $0.60 \mu_B/f.u.$ and is an estimate of M_{sat} at 0 K, which, for a simple ferromagnet, corresponds to the spontaneous moment M_0 of the ordered state. The scaled Arrott analysis is consistent with the Curie-Weiss analysis,

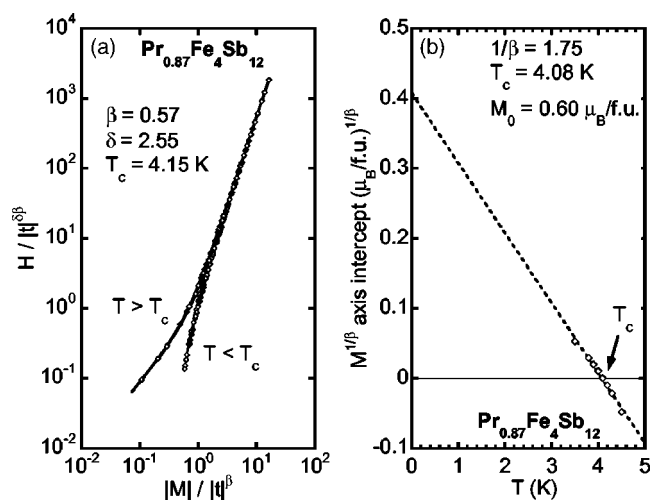


FIG. 5. (a) Collapse of magnetization isotherms onto two curves, for T above and below the magnetic ordering temperature T_c , indicating the chosen scaling exponents. (b) $M^{1/\beta}$ intercepts from the scaled Arrott plot (Fig. 4) demonstrate linear spacing in T , with $T_c = 4.08$ K. A linear extrapolation to $T = 0$ K yields a value $M_0 = 0.60 \mu_B/f.u.$

which can be seen by the proximity of the $|H/M|^{1/\gamma}$ intercepts (raised to the γ power) to the extrapolated Curie-Weiss fit (inset of Fig. 2).

C. Neutron diffraction

Neutron-diffraction measurements were performed on two single crystals to investigate the magnetic phase transition and magnetic structure of $\text{Pr}_{0.87}\text{Fe}_4\text{Sb}_{12}$. No half-integral type magnetic peaks were observed, establishing that the magnetic and chemical unit cells are identical. Because all of the magnetic peaks coincide with structural (nuclear) peaks, the magnetic signal was determined by measuring the change in the intensities of the Bragg peaks above and below the magnetic transition. Figure 6 illustrates the temperature dependence of the (110) nuclear Bragg peak, which has a particularly weak intensity that provides the best ratio of magnetic to nuclear intensity. The solid curve is a fit using power law and provides an estimate of 4.22(8) K for the ordering temperature. The statistical uncertainties in the neutron work represent one standard deviation.

Determination of the detailed magnetic structure requires measurement of the magnetic intensities of a series of inequivalent peaks, and generally the magnetic intensity at each peak can be identified by subtracting the nuclear intensity observed above the transition.²⁶ In the case of $\text{Pr}_{0.87}\text{Fe}_4\text{Sb}_{12}$, however, the magnetic intensities are weak—typically they are only a few percent or less of the nuclear peak intensities. The subtraction technique requires that the nuclear intensities do not change significantly above and below the transition, and small shifts of the atomic positions through magnetoelastic coupling might affect the nuclear intensities at the level of precision needed in this case. The experimental data collection was further complicated by the irregular mosaic structure of the first crystal investigated,

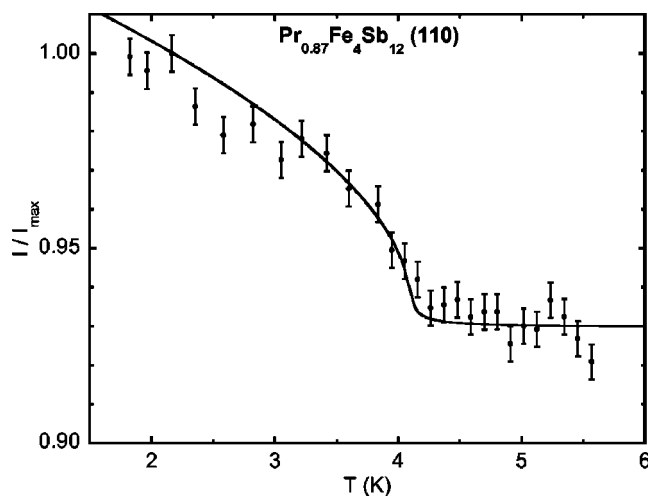


FIG. 6. Neutron-diffraction intensity of the (110) peak, indicating the onset of magnetic ordering around 4 K. The curve is a power-law fit to the data.

which prevented an accurate experimental determination of the relative intensities of both the magnetic and structural Bragg peaks. It has been necessary to rely on a calculation of each nuclear structure factor to put the (subtracted) magnetic intensity on the appropriate relative scale, and this introduces additional systematic uncertainties. The large Debye-Waller factor for the “rattling” Pr ion in the filled skutterudite structure can also introduce systematic uncertainties even at the low temperatures at which measurements were performed, particularly for peaks at larger reciprocal lattice vectors. In an attempt to avoid the problems associated with the mosaic spread of the first crystal investigated, data were also collected on a small crystal with a single-peaked mosaic, but due to the reduced signal, the statistical uncertainties were too large to be useful. Finally, it should be noted that polarized neutron scattering could potentially be used to unambiguously identify the magnetic scattering, but the loss of intensity associated with this procedure precluded its use in the present study.

Despite these experimental difficulties, considerable information has been determined about the magnetic structure, although it was not possible to achieve a complete solution. Figure 7 shows the normalized integrated intensities (solid circles) determined as a function of wave vector. The solid curve represents the square of the Pr form factor (green online) and the dashed curve represents the square of the Fe magnetic form factor (red online). The observed intensities split into two classes of reflections, strong and weak, with an overall trend of the intensities decreasing with increasing wave vector, as expected for magnetic scattering.

To analyze these data, a number of magnetic structure factor calculations have been performed. To begin with, it might be assumed that only the Pr ions carry a moment. A ferromagnetic (FM) configuration would then give the correct peak positions, but all magnetic reflections would have the same magnetic structure factor, because of the special position in the unit cell that the Pr ions occupy, and therefore the only intensity change would be due to the magnetic form

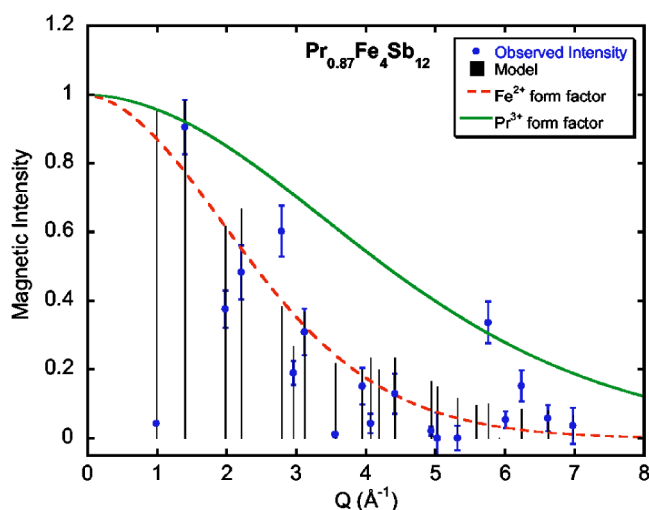


FIG. 7. (Color online). Solid blue circles are the observed integrated magnetic intensities. The black vertical lines represent a magnetic model that involves an AFM alignment of Fe spins and a FM alignment of Pr spins. The solid green curve and the dashed red curve are the square of the Pr and Fe magnetic form factors, respectively, for comparison purposes.

factor, contrary to the experimental observations. In addition, the absence of $h+k+l=2N+1$ peaks rules out collinear commensurate antiferromagnetic (AFM) ordering of the Pr ions alone. The Fe ions also occupy special positions, and an assumption that only the Fe ions carry a moment leads to the same inconsistencies described for the case of Pr moments. It is therefore probable that both Pr and Fe ions have an ordered moment, and the magnetic structure is more complicated. Calculations were made for simple collinear magnetic configurations of both moments, leading to the following conclusions. Of all possible AFM Fe spin configurations, only two have no reflections at the $h+k+l=2N+1$ forbidden locations. Another possibility is a FM Fe configuration, coupled ferrimagnetically (antiparallel) to the Pr sublattice, and these three Fe spin configurations are candidates for a simple collinear magnetic model. Taken alone, the three Fe spin configurations generate peaks at even indexed $(2h, 2k, 2l)$ locations only. Any one of the three Fe spin configurations, coupled to a FM Pr spin configuration, results in a model that predicts peaks at all the locations observed. However, the agreement is only semiquantitative, as shown in Fig. 7 (black vertical lines). One important discrepancy is that all these models predict substantially more intensity than is observed at the (110) magnetic peak, where the order parameter was measured. More complicated models could be tried, but it is unlikely that a unique model could be identified given the experimental difficulties. Thus, more definitive results must await the availability of higher quality single crystals.

D. Specific heat

The specific heat of $\text{Pr}_{0.87}\text{Fe}_4\text{Sb}_{12}$, shown in Fig. 8, was measured from $0.6 \text{ K} \leq T \leq 82 \text{ K}$. The main low-temperature feature is a hump that can be associated with the onset of

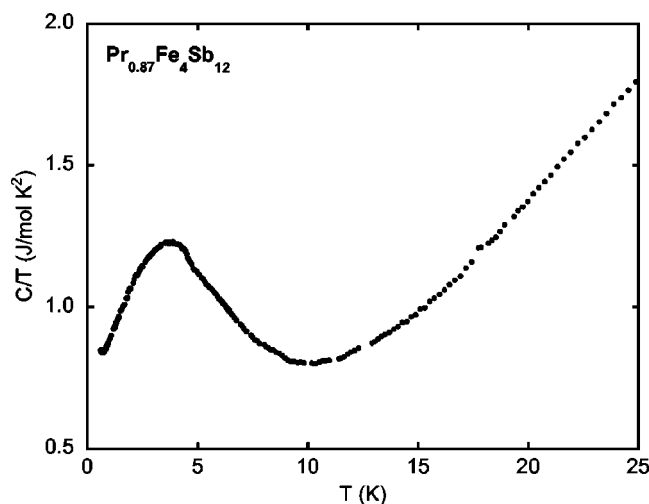


FIG. 8. The specific heat divided by temperature vs T . The magnetic transition is associated with the broad peak centered at ~ 4 K.

magnetic order when considered along with the $\chi_{ac}(T)$ and $M(H)$ measurements described earlier. It is important to note that the hump in C/T vs T is not as well defined as that expected for a typical ferromagnetic transition and is too wide to be due to a distribution of critical temperatures. Overall, the C/T vs T data for $\text{Pr}_{0.87}\text{Fe}_4\text{Sb}_{12}$ single crystals resemble the results obtained for polycrystals by Bauer *et al.*²² The magnitude of the low-temperature specific-heat data is a strong indication of an enhanced electronic contribution to the specific heat and is a possible indication of heavy-fermion behavior. However, absolute confirmation of a large electronic contribution is complicated by the persistence of the broad hump to lowest measured T and by the difficulty in assigning a crystalline electric field (CEF) energy level splitting scheme, which is discussed in more detail in the CEF section. It should be noted that the studies by Bauer *et al.* of polycrystalline $\text{Pr}_{0.73}\text{Fe}_4\text{Sb}_{12}$ revealed the existence of a Pr nuclear Schottky anomaly at $T < 1$ K,²² making absolute confirmation of the magnitude of the electronic specific heat a difficult prospect. Inability to accurately determine the electronic contribution to $C(T)$ makes isolation of the magnetic component tenuous. The resonance level model of Schotte and Schotte²⁷ has been used to estimate the electronic specific heat in other Pr-based filled skutterudites, but it is an approximate single-ion model and was not applied in this case.

E. Electrical resistivity

The electrical resistivity $\rho(T)$ of several $\text{Pr}_{0.87}\text{Fe}_4\text{Sb}_{12}$ single crystals was measured. Figure 9 displays the temperature dependence of the resistivity of a representative sample at $H=0$ T and pressure $P=1$ atm. The resistivity monotonically increases with temperature, with a gradual decrease in $\partial\rho/\partial T$ until ρ is linear in T by ~ 200 K, which persists to 300 K. One particular feature stands out: the change in $\partial\rho/\partial T$ at ~ 10 K. Because this feature occurs at a significantly higher temperature than T_c , it could indicate that weak

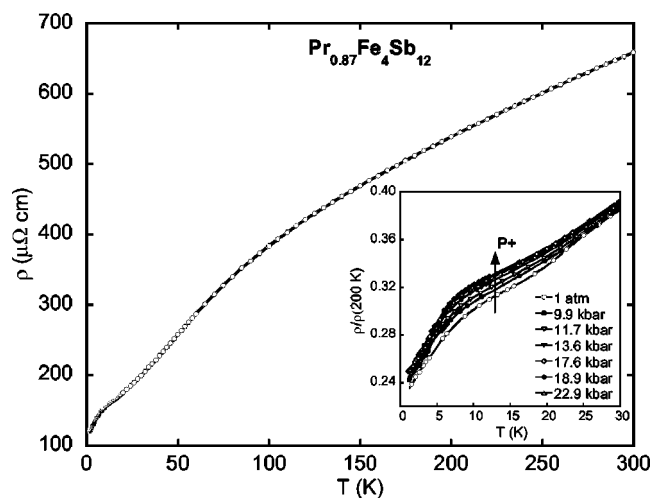


FIG. 9. Electrical resistivity $\rho(T)$ at field $H=0$ T and pressure $P=1$ atm. $\text{Pr}_{0.87}\text{Fe}_4\text{Sb}_{12}$ exhibits little H or P dependence over most of this temperature range. The inset shows $\rho(T, P)$ at low T . There is a change in $\partial\rho/\partial T$ at ~ 10 K for all measured P .

magnetic correlations persist up to 10 K, leading to a broad transition in $C_p(T)$, with the drop in $\rho(T)$ due to reduced spin-flip scattering below 10 K. Above 50 K, $\rho(T)$ is insensitive to applied pressure P , changing by $< 5\%$. Below ~ 30 K, some P dependence is evident (inset of Fig. 9), but changes in the value of $\rho(T)$ are not very large, nor are changes in $\partial\rho/\partial T$.

It is also apparent that ρ is weakly dependent on H , with a decrease in $\rho(T)$ of only $\sim 15 \mu\Omega \text{ cm}$ between 20 and 300 K at $H=9$ T and little perceptible change in the curvature of $\rho(T)$. However, the magnetic ordering transition can be observed in $\rho(H, T)$ as the sign of $\partial\rho/\partial H$ changes as T is raised through T_c (not shown). This same behavior appears more dramatically in $\rho(T)$, as illustrated in Fig. 10(a). For $T \leq 2.6$ K, $\rho(T)$ exhibits a power-law T dependence that can be expressed as $\rho(T) = \rho_0 + AT^n$ with residual resistivity $\rho_0 = \rho(0 \text{ K})$, a power law coefficient A , and exponent n (Fig. 11). In low applied field, $0 \text{ T} \leq H \leq 10 \text{ T}$, ρ_0 increases with H , but for $H > 10 \text{ T}$, $\rho_0 \approx 127 \mu\Omega \text{ cm}$. The dependence of ρ_0 and the exponent n on H is shown in Fig. 10(b), as n decreases for $2 \text{ T} \leq H \leq 10 \text{ T}$ and then reaches a value of ~ 2 in highest fields. Attempts to fit the data to curves of the form $\rho(T) = \rho_0 + AT^n \exp(-\Delta/k_B T)$, where Δ is a spin wave energy gap, resulted in worse fits than to the bare power law, and yielded exponents n that still had significant H dependence. Studies of polycrystalline $\text{Pr}_{0.73}\text{Fe}_4\text{Sb}_{12}$ led to the interpretation of this behavior as evidence of the absence of long-range magnetic order at intermediate fields.^{21,22}

F. Crystalline electric field

To determine the crystalline electric field (CEF) splitting scheme for the Pr^{3+} ion in $\text{Pr}_{0.87}\text{Fe}_4\text{Sb}_{12}$, attempts were made to fit curves derived from CEF calculations to $\chi_{dc}^{-1}(T)$ and $\rho(T)$ data. The analysis was simplified by assuming cubic O_h symmetry for $\text{PrFe}_4\text{Sb}_{12}$ rather than the actual tetrahedral

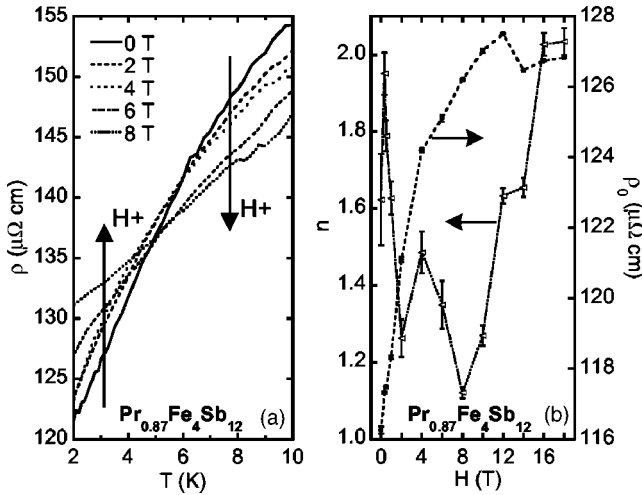


FIG. 10. (a) Electrical resistivity $\rho(T, H)$ at low T . There is a change in sign of $\partial\rho/\partial H$ as T sweeps through the magnetic ordering transition. (b) Exponents and ρ intercepts from power-law fits to low T $\rho(T)$ (Fig. 11). The exponent goes through a minimum as H increases to 18 T, while ρ_0 saturates above 8 K.

symmetry T_h ,²⁸ as the extra term primarily affects the matrix elements rather than the crystal field energies.²⁹ The cubic CEF splits the nine fold degenerate $\text{Pr}^{3+}J=4$ multiplet into a Γ_1 singlet, Γ_3 doublet, Γ_4 triplet, and Γ_5 triplet. When fitting to $\text{Pr}_{0.87}\text{Fe}_4\text{Sb}_{12}$ data, a Γ_5 ground state was always assumed because Γ_5 is the only allowed magnetic ground state for an O_h CEF split $J=4$ multiplet. Following the method used by Lea, Leask, and Wolf (LLW), x and W values (where x is the ratio of the fourth- and sixth-order terms of the angular momentum operators and W is an overall energy scale) are used to describe a set of energy levels.³⁰

Because the calculated μ_{eff} has a contribution from the $\text{Fe}_4\text{Sb}_{12}$ sublattice, analysis of the magnetic susceptibility data first required subtraction of the contribution to the effective moment $\mu_{\text{eff}}^{\text{Fe}_4\text{Sb}_{12}}$. The value of $\mu_{\text{eff}}^{\text{Fe}_4\text{Sb}_{12}}$ was derived

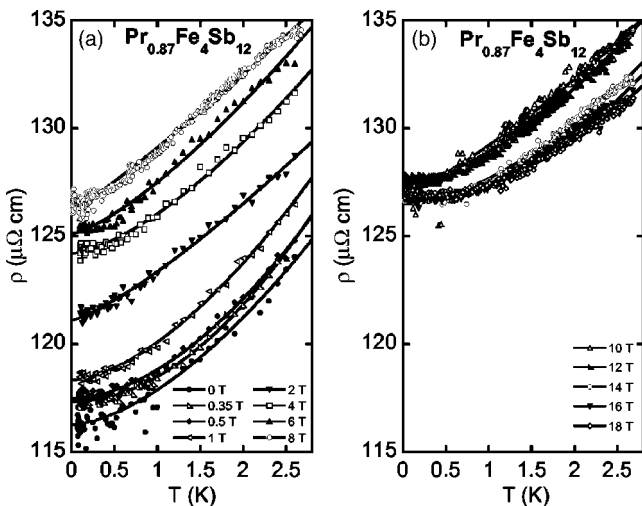


FIG. 11. (a),(b) Power-law fits to low-temperature electrical resistivity $\rho(T)$ for various fields H up to 18 T, separated for clarity. Fit parameters are plotted in Fig. 10(b).

under the assumption that the Pr^{3+} moment $\mu_{\text{eff}}^{\text{Pr}}$ and the $\text{Fe}_4\text{Sb}_{12}$ sublattice moment $\mu_{\text{eff}}^{\text{Fe}_4\text{Sb}_{12}}$ are additive and are described by the same Curie-Weiss law. Although both paramagnetic species need not generally have the same θ_{CW} , in $\text{Pr}_{0.87}\text{Fe}_4\text{Sb}_{12}$ their magnitudes can not be much larger than 4 K, or one of the species would have ordered at temperatures higher than T_c . Considering the wide temperature range over which the Curie-Weiss law is applicable (Fig. 1), it is reasonable to treat the high-temperature paramagnetic moments in this manner, and it certainly agrees with the observation that both magnetic species order below T_c . Thus, $\mu_{\text{eff}}^{\text{meas}}$ is given by

$$\mu_{\text{eff}}^{\text{meas}} = \sqrt{f^{\text{Pr}}(\mu_{\text{eff}}^{\text{Pr}})^2 + (\mu_{\text{eff}}^{\text{Fe}_4\text{Sb}_{12}})^2} \quad (1)$$

with $\mu_{\text{eff}}^{\text{meas}} = 4.34\mu_B$, filling fraction $f^{\text{Pr}} \approx 0.87$ determined via x-ray refinement, and assuming that $\mu_{\text{eff}}^{\text{Pr}}$ is equal to the theoretical Pr^{3+} free ion moment ($\mu_{\text{eff}} = 3.58\mu_B$). Equation (1) yields $\mu_{\text{eff}}^{\text{Fe}_4\text{Sb}_{12}} = 2.77\mu_B$, comparable to a value determined by Bauer and co-workers.²² Subtraction of a Curie-Weiss law susceptibility with $\mu_{\text{eff}}^{\text{Fe}_4\text{Sb}_{12}} = 2.77\mu_B$ from the H/M data results in a susceptibility curve representing only the Pr^{3+} contribution. This curve was rescaled to correct for partial filling and the corrected magnetic susceptibility χ_{Pr} was fit to $\chi_{\text{Pr}}^{-1} = \chi_{\text{CEF}}^{-1} - \lambda$, which includes a molecular field parameter λ due to the presence of magnetic order in $\text{Pr}_{0.87}\text{Fe}_4\text{Sb}_{12}$.

In order to analyze the $\rho(T)$ data it was necessary to calculate a lattice contribution ρ_{lat} , an impurity contribution ρ_{imp} ($\sim 115 \mu\Omega \text{ cm}$), and a contribution due to s - f exchange scattering ρ_{mag} from the $\text{Pr}^{3+} 4f$ energy levels in a cubic CEF. The lattice contribution was determined from the isostructural nonmagnetic compound $\text{LaFe}_4\text{Sb}_{12}$, although it could not be used above 100 K where $\rho(T)$ of $\text{LaFe}_4\text{Sb}_{12}$ exhibits significant negative curvature, a common feature of La-based compounds.^{31,32} Alternative candidates for estimation of the lattice background are $\text{YFe}_4\text{Sb}_{12}$ and $\text{LuFe}_4\text{Sb}_{12}$, which may have less pronounced curvature in $\rho(T)$, but have not yet been prepared, to our knowledge. The impurity contribution ρ_{imp} was estimated from the low-temperature $\rho(T)$ data (Fig. 11). The contribution due to exchange scattering ρ_{mag} was calculated for splitting of the Hund's rule $J=4$ multiplet of Pr^{3+} in a cubic CEF, similar to a method described elsewhere for $\text{PrOs}_4\text{Sb}_{12}$ (Ref. 33) and based on work by Andersen *et al.*³⁴ Addition of an aspherical Coulomb scattering contribution to the fit of the $\rho(T)$ data did not improve the quality of the CEF fits. The final fit to the $\rho(T)$ data up to 100 K took the form $\rho = \rho_{\text{lat}} + \rho_{\text{imp}} + \rho_{\text{mag}}$.

Fits to the $\chi_{\text{Pr}}^{-1}(T)$ and $\rho(T)$ data using the various energy level schemes with a Γ_5 ground state were indistinguishable and a single best energy level scheme could not be determined. However, the splittings between the various energy levels for each scheme were comparable. Reasonable fits to the $\chi_{\text{Pr}}^{-1}(T)$ and $\rho(T)$ data for $10 \text{ K} \leq T \leq 100 \text{ K}$ were obtained with the following x and W values in the three regions of the x - W plane with a Γ_5 ground state: $(x, W) = (-0.93, -5.0)$, $(0.69, 3.8)$, and $(1.0, 4.3)$. The calculated energy level splittings were on the order of 70-130 K between the ground state and the first excited state, 130-180 K between the ground state and second excited state, and 180-270 K be-

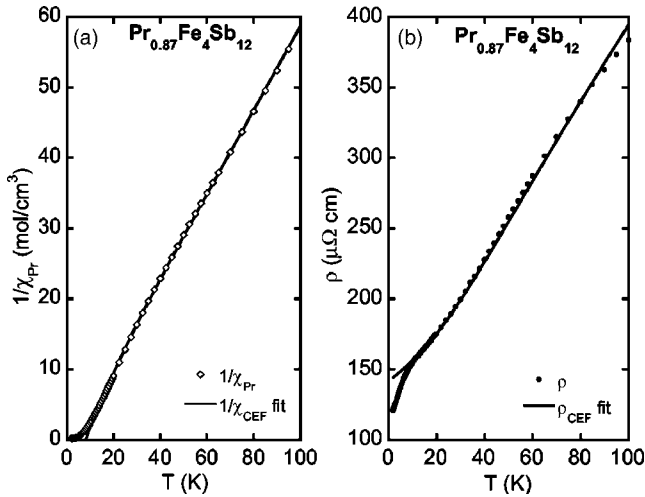


FIG. 12. (a) A representative CEF fit to the inverse magnetic susceptibility, after subtraction of the $\text{Fe}_4\text{Sb}_{12}$ contribution and correction for partial filling. (b) A representative CEF fit to the electrical resistivity, which includes lattice, impurity, and magnetic contributions.

tween the ground state and the third excited state. Due to the similarity of the various CEF fits, one representative set $(x, W) = (-0.93, -5.0)$, was chosen for display in Fig. 12(a). This corresponds to the energy level scheme: Γ_5 ground state, Γ_3 at 110 K, Γ_4 at 177 K, and Γ_1 at 272 K. It can be seen that the $\chi_{\text{Pr}}^{-1}(T)$ data are almost featureless except for a slight curvature that occurs around 20-30 K, which is fit quite well with the energy splittings described above along with a molecular field parameter $\lambda \sim 7.65 \text{ mol/cm}^3$. Figure 12(b) shows the $\rho(T)$ data, which also do not exhibit many features between 10 and 100 K. A reasonable CEF fit to the $\rho(T)$ data was obtained when using the energy splittings described earlier in addition to a lattice contribution of 1.57 times that due to $\text{LaFe}_4\text{Sb}_{12}$ and an impurity contribution of $115 \mu\Omega \text{ cm}$. The range of CEF splittings determined for single crystals of $\text{Pr}_{0.87}\text{Fe}_4\text{Sb}_{12}$ is comparable to those calculated for polycrystalline $\text{Pr}_{0.73}\text{Fe}_4\text{Sb}_{12}$, although Bauer and co-workers identified features in $M(T)$ that were important for determining the CEF splitting,²² which were not observed in $M(T)$ for the single crystals.

In this study, difficulties in determining a unique best CEF fit to the data arose for three main reasons. First, the lattice contribution to the $\rho(T)$ data is not known accurately above 100 K, limiting the range of the CEF fits to the $\rho(T)$ data. Second, the $\chi_{\text{Pr}}^{-1}(T)$ and $\rho(T)$ data from 10-100 K exhibit few features that would allow one to discriminate between different sets of CEF fitting parameters. The data are so featureless that a fit that does not include CEF splitting is barely distinguishable from one that does. The final difficulty in determining a single CEF scheme is the absence of a Schottky anomaly in the $C(T)$ data.

IV. DISCUSSION

Although there are several unusual features in the bulk physical properties of $\text{Pr}_{0.87}\text{Fe}_4\text{Sb}_{12}$, a consistent picture

emerges when they are considered along with the neutron-diffraction data. One detail that makes characterization of the bulk magnetization difficult is the lack of obvious saturation of $M(H)$. The situation is complicated by the curvature of $M(H)$, which makes estimation of the saturation magnetization M_{sat} directly from $M(H)$ difficult. Although the $M(H)$ curves bear superficial resemblance to Brillouin functions, the data exhibit too much curvature at high fields and attempts to subtract a Brillouin contribution were unsatisfactory, as were all attempts to estimate a paramagnetic contribution to the magnetization below T_c . This failure is consistent with the fact that ordering is observed on both the Pr and Fe sites in neutron diffraction. A simple estimate of M_{sat} is the magnetization at which $M(H)$ at low T ceases to be hysteretic, or $\sim 0.3\mu_B/\text{f.u.}$ (inset of Fig. 3). This value does not agree closely with the estimate of $M_{\text{sat}} = 0.60\mu_B/\text{f.u.}$ that was linearly extrapolated from the $M^{1/\beta}$ intercepts of the modified Arrott plot [Fig. 5(b)], but the applicability of that extrapolation is questionable. Nonetheless, it is clear that either estimate of M_{sat} is far from the limiting value of the magnetization, which is at least $\sim 2.6\mu_B/\text{f.u.}$ measured at $H=15 \text{ T}$ by Bauer and co-workers, whose $M(H)$ data exhibit nonlinearity through 15 T.²² Interestingly, the value of $0.60\mu_B/\text{f.u.}$ is close to the magnitude of M at $H_{\chi} \approx 0.5 \text{ T}$ (Fig. 3), the field at which the measured $M(H)$ isotherms coincide for $T < T_c$.

Unlike some compounds, such as the filled skutterudite $\text{NdOs}_4\text{Sb}_{12}$, where the saturated moment is accounted for entirely by the expected CEF-split ground state moment,³ $\text{Pr}_{0.87}\text{Fe}_4\text{Sb}_{12}$ has an ordered moment that cannot be explained fully by CEF splitting. For $\text{Pr}_{0.87}\text{Fe}_4\text{Sb}_{12}$, the Γ_5 ground state should contribute $2\mu_B/\text{f.u.}$, while in this study $M(5.5 \text{ T}) = 1.65\mu_B/\text{f.u.}$ and Bauer *et al.* reported $M(15 \text{ T}) \approx 2.6\mu_B/\text{f.u.}$ ²² These values suggest a contribution to the magnetization besides that of the Pr, consistent with an ordered moment arising from the $\text{Fe}_4\text{Sb}_{12}$ sublattice.

The small value of the estimated M_{sat} of $\text{Pr}_{0.87}\text{Fe}_4\text{Sb}_{12}$ has further implications. A comparison of M_{sat} with the paramagnetic effective moment of $4.3\mu_B/\text{f.u.}$ yields a ratio $\mu_{\text{eff}}/M_{\text{sat}}$ of ~ 7 , an indication of weak ferromagnetism in conventional FM systems.^{35,36} Small ordered moments are often the hallmark of itinerant magnetism, which is characterized by persistent spin fluctuations above the ordering temperature T_c . This notion is compatible with the drop in $\rho(T)$ at $\sim 10 \text{ K}$, the broad magnetic $C_p(T)$ peak, and the unsaturated high-field moment observed in $\text{Pr}_{0.87}\text{Fe}_4\text{Sb}_{12}$. Because of the strong tendency toward local moment behavior of Pr f electrons and the large Pr-Sb interatomic spacing in $\text{Pr}_{0.87}\text{Fe}_4\text{Sb}_{12}$ (Table I), an itinerant moment would be expected to arise from the $\text{Fe}_4\text{Sb}_{12}$ sublattice. This presumption is bolstered by reports that band structure calculations and measurements of $\text{NaFe}_4\text{Sb}_{12}$ and $\text{KFe}_4\text{Sb}_{12}$ have indicated the existence of itinerant ferromagnetism,³⁷ and that spin-polarized band structure calculations for $\text{LaFe}_4\text{Sb}_{12}$ yielded a magnetic solution.³⁸

The aforementioned features of $M(H, T)$ of $\text{Pr}_{0.87}\text{Fe}_4\text{Sb}_{12}$ are consistent with a ferrimagnetic arrangement of Pr and Fe magnetic sublattices. It is compelling that both neutron scattering and bulk magnetization data indicate the existence of

Pr and Fe ordered moments. A quick calculation using Eq. (1) further supports the existence of ferrimagnetism. In this case, $\mu_{\text{eff}}^{\text{meas}}=4.13\mu_B$ from the low- T Curie-Weiss law fit (Fig. 2), Pr filling fraction $f^{\text{Pr}}\approx 0.87$, and assuming that $\mu_{\text{eff}}^{\text{Pr}}$ is due to the Pr³⁺ cubic CEF-split Γ_5 ground state ($\mu_{\text{eff}}^{\text{Pr}}=2.83\mu_B$), $\mu_{\text{eff}}^{\text{Fe}_4\text{Sb}_{12}}=3.18\mu_B$. The paramagnetic moment is related to the spin by $(\mu_{\text{eff}}^{\text{Fe}_4\text{Sb}_{12}})^2=g^2J(J+1)$, with $g=2$ for Fe, yielding an effective spin of 1.17 for the Fe₄Sb₁₂ sublattice. The Fe saturated moment $\mu_{\text{sat}}^{\text{Fe}_4\text{Sb}_{12}}=gJ=2.33\mu_B$, while for the Pr³⁺ Γ_5 ground state, $\mu_{\text{sat}}^{\text{Pr}}=2\mu_B$ and correction for partial filling results in $\mu_{\text{sat}}^{\text{Pr}}=1.74\mu_B$. An antiparallel arrangement of the Pr and Fe sublattices yields a moment of $0.59\mu_B$, while a parallel arrangement has a moment of $4.07\mu_B$. In the ferrimagnetic state, M would increase from $0.59\mu_B$ to $4.07\mu_B$ with increasing applied field, as one of the magnetic sublattices aligns with H . The case of Pr_{0.87}Fe₄Sb₁₂ could be complicated by the itinerant nature of the Fe moment, which may be responsible for the curvature in $M(H)$ and the absence of saturation in high field. The moment realignment may also cause the field dependence of the power-law exponents observed in the low-temperature resistivity of Pr_{0.87}Fe₄Sb₁₂ [Fig. 10(b)] for applied fields between 0.5 and 10 T. As the magnetic structure reorients under the influence of the external magnetic field, the excitation spectrum of magnons in the compound would be expected to alter, influencing electron-magnon scattering at low temperatures.

It should also be noted that for systems with rare earth constituents, an alternative explanation for weak magnetic moments may be Kondo screening, which has been suggested for the compounds Yb_{0.8}Y_{0.2}InCu₄ (Ref. 39) and SmFe₄P₁₂.² It is not clear what role screening plays in Pr_{0.87}Fe₄Sb₁₂, however, because $\rho(T)$ does not display the characteristic Kondo-lattice shoulder, and $M(T)$ follows a Curie-Weiss law down to 20 K, below which there are no indications of moment screening through T_c .

Another peculiar property of the compound Pr_{0.87}Fe₄Sb₁₂ is the values of its critical exponents $\beta=0.57$, $\gamma=0.884$, and $\delta=2.55$. In particular, for Pr_{0.87}Fe₄Sb₁₂ the best-fit value for γ is less than 1, whereas most theories and experiments report values greater than 1, regardless of the ordered state.^{40–46} Artificially forcing $\gamma\geq 1$ results in $H/|t|^{\delta\beta}$ vs $|M|/|t|^\beta$ plots of significantly lower quality. It is interesting that despite differences in both rare-earth and transition metal constituents, the magnetic behavior of Pr_{0.87}Fe₄Sb₁₂ is similar to that of SmOs₄Sb₁₂.⁴⁷ The critical exponents of SmOs₄Sb₁₂ are comparable ($\beta=0.73$, $\gamma=0.60$, and $\delta=1.82$) and SmOs₄Sb₁₂ also exhibits a magnetization that does not saturate in high H . Unfortunately, the magnetic structure of SmOs₄Sb₁₂ has not been determined. Furthermore, this unusual magnetic behavior is not observed in all filled skutterudites. In contrast to the previous two compounds, the magnetic transition in NdOs₄Sb₁₂ is described by critical exponents consistent with mean-field ferromagnetism.³

Among the filled skutterudite compounds, SmFe₄Sb₁₂, EuFe₄Sb₁₂, NdFe₄Sb₁₂, and PrFe₄Sb₁₂ have effective paramagnetic moments larger than the theoretical free ion values of their rare-earth constituents.²⁰ Moreover, a study of EuFe₄Sb₁₂ suggested ferrimagnetic ordering as a

possibility in that compound.⁴⁸ While there is evidence that the Fe₄Sb₁₂ sublattices of EuFe₄Sb₁₂, NdFe₄Sb₁₂, and PrFe₄Sb₁₂ contribute to the unusual magnetic ordering of those compounds, the Fe₄Sb₁₂ sublattice may not always order magnetically. In fact, the magnetic order in SmFe₄Sb₁₂ has been attributed exclusively to Sm³⁺.²⁰ Although Bauer and co-workers have reported that ferromagnetic ordering in NdFe₄Sb₁₂ has been determined by neutron diffraction,²¹ a study of the critical behavior of the bulk magnetization of NdFe₄Sb₁₂ might establish whether NdFe₄Sb₁₂, and PrFe₄Sb₁₂ have some unusual common features that could explain their magnetic properties. Spin-polarized band structure calculations may also establish the possibility of itinerant magnetism in these systems.

Because there are strong indications that the ordered state of PrFe₄Sb₁₂ consists of both local and itinerant moments, accurate theoretical treatment might not be accomplished until the precise nature of the ordering is determined experimentally. Although this would require the growth of large, high-quality crystals, which is nontrivial, it would also be beneficial to perform inelastic neutron-scattering measurements on PrFe₄Sb₁₂ to confirm CEF energy splitting and to establish the exponents ν and η [correlation length $\xi\sim t^{-\nu}$ and correlation function $G(q)\sim q^{-2+\nu}$ for wave vector q], which could be used to verify β , γ , and δ via hyperscaling relations.

V. SUMMARY

Long-range magnetic ordering has been demonstrated in single-crystalline Pr_{0.87}Fe₄Sb₁₂ by both neutron-diffraction and modified Arrott plot analysis. Magnetic ordering on both Pr and Fe sites was identified, indicating a complex, possibly ferrimagnetic, structure that is consistent with bulk properties. The broad peak in the specific heat, shoulder in the electrical resistivity data at ~ 10 K, lack of saturation in $M(H)$, and large value of $\mu_{\text{eff}}/M_{\text{sat}}$ all suggest the presence of an itinerant moment. The observed magnetic critical exponents $\beta=0.57$, $\gamma=0.884$, and $\delta=2.55$ bear some similarity to those of SmOs₄Sb₁₂, but differ significantly from many reported magnetic systems and cannot be adequately explained by classical or quantum critical models. The resistivity of Pr_{0.87}Fe₄Sb₁₂ is notably insensitive to applied field and pressure over most of the measured temperature range. Although the magnitude of the specific heat at low temperatures indicates electronic mass enhancement, it has been difficult to isolate the electronic contribution and precisely determine the value of the effective mass. A unique CEF scheme cannot be assigned to the Pr³⁺ ion because of the featureless magnetic susceptibility and resistivity, and the large hump in specific heat. Conclusively determining the magnetic structure and dynamics of PrFe₄Sb₁₂, which would require the growth of larger, high-quality single crystals, may shed light on the relationship between localized and itinerant magnetic critical behavior. Further elastic and inelastic neutron-scattering studies of PrFe₄Sb₁₂ are warranted.

ACKNOWLEDGMENTS

We thank S. K. Kim, E. D. Bauer, and L. N. Zakharov for experimental assistance and C. Capan for technical support at NHMFL at Los Alamos. X. G. Zheng thanks Saga University for supporting his stay at UCSD. Research at UCSD was supported by the National Nuclear Security Administration under the Stewardship Science Academic Alliances program

through DOE Research Grant No. DE-FG52-03NA00068 and by the National Science Foundation (NSF) under Research Grant No. DMR 0335173. The work at the NHMFL Pulsed Field Facility (Los Alamos National Laboratory) was performed under the auspices of the NSF, the State of Florida and the US Department of Energy. Identification of commercial equipment in the text is not intended to imply recommendation or endorsement by the National Institute of Standards and Technology.

*Permanent address: Department of Physics, Saga University, Japan

- ¹N. R. Dilley, E. J. Freeman, E. D. Bauer, and M. B. Maple, *Phys. Rev. B* **58**, 6287 (1998).
- ²N. Takeda and M. Ishikawa, *J. Phys.: Condens. Matter* **15**, L229 (2003).
- ³P.-C. Ho, W. M. Yuhasz, N. P. Butch, N. A. Frederick, T. A. Sayles, J. R. Jeffries, M. B. Maple, J. B. Betts, A. H. Lacerda, P. Rogl, and G. Giester, cond-mat/0412713 (unpublished).
- ⁴E. D. Bauer, A. Ślebarski, E. J. Freeman, C. Sirvent, and M. B. Maple, *J. Phys.: Condens. Matter* **13**, 4495 (2001).
- ⁵G. P. Meisner, *Physica B & C* **108**, 763 (1981).
- ⁶W. Jeitschko and D. Braun, *Acta Crystallogr., Sect. B: Struct. Crystallogr. Cryst. Chem.* **33**, 3401 (1977).
- ⁷C. Sekine, T. Uchiumi, I. Shirovani, and T. Yagi, *Phys. Rev. Lett.* **79**, 3218 (1997).
- ⁸M. Matsunami, L. Chen, H. Okamura, T. Nanba, C. Sekine, and I. Shirovani, *J. Magn. Magn. Mater.* **272-276**, E39 (2004).
- ⁹N. Takeda and M. Ishikawa, *J. Phys. Soc. Jpn.* **69**, 868 (2000).
- ¹⁰K. Abe, H. Sato, T. D. Matsuda, T. Namiki, H. Sugawara, and Y. Aoki, *J. Phys.: Condens. Matter* **14**, 11757 (2002).
- ¹¹M. Yogi, H. Kotegawa, Y. Imamura, G.-q. Zheng, Y. Kitaoka, H. Sugawara, and H. Sato, *Phys. Rev. B* **67**, 180501(R) (2003).
- ¹²I. Shirovani, T. Uchiumi, K. Ohno, C. Sekine, Y. Nakazawa, K. Kanoda, S. Todo, and T. Yagi, *Phys. Rev. B* **56**, 7866 (1997).
- ¹³E. D. Bauer, N. A. Frederick, P.-C. Ho, V. S. Zapf, and M. B. Maple, *Phys. Rev. B* **65**, 100506(R) (2002).
- ¹⁴M. B. Maple, P.-C. Ho, V. S. Zapf, N. A. Frederick, E. D. Bauer, W. M. Yuhasz, F. M. Woodward, and J. W. Lynn, *J. Phys. Soc. Jpn.* **71**, 23 (2002).
- ¹⁵M. S. Torikachvili, J. W. Chen, Y. Dalichaouch, R. P. Guertin, M. W. McElfresh, C. Rossel, M. B. Maple, and G. P. Meisner, *Phys. Rev. B* **36**, 8660 (1987).
- ¹⁶Y. Aoki, T. Namiki, T. D. Matsuda, K. Abe, H. Sugawara, and H. Sato, *Phys. Rev. B* **65**, 064446 (2002).
- ¹⁷H. Sugawara, T. D. Matsuda, K. Abe, Y. Aoki, H. Sato, S. Nojiri, Y. Inada, R. Settai, and Y. Lnuiki, *Phys. Rev. B* **66**, 134411 (2002).
- ¹⁸N. A. Frederick, T. D. Do, P.-C. Ho, N. P. Butch, V. S. Zapf, and M. B. Maple, *Phys. Rev. B* **69**, 024523 (2004).
- ¹⁹Y. Nakanishi, T. Kumagai, M. Oikawa, T. Kanayama, Y. Aoki, H. Sugawara, H. Sato, and M. Yoshizawa, *Physica B* **346-347**, 142 (2004).
- ²⁰M. E. Danebrock, C. B. H. Evers, and W. Jeitschko, *J. Phys. Chem. Solids* **57**, 381 (1996).
- ²¹E. Bauer, St. Berger, A. Galatanu, Ch. Paul, M. Della Mea, H. Michor, G. Hilscher, A. Grytsiv, P. Rogl, D. Kaczorowski, L. Keller, T. Hermannsdörfer, and P. Fischer, *Physica B* **312-313**, 840 (2002).
- ²²E. Bauer, St. Berger, Ch. Paul, M. D. Mea, G. Hilscher, H. Michor, M. Reissner, W. Steiner, A. Grytsiv, P. Rogl, and E. W. Scheidt, *Phys. Rev. B* **66**, 214421 (2002).
- ²³NONIUS KAPPA CCD package, COLLECT, DENZO, SCALEPACK, SORTAV, Nonius Delft, The Netherlands, 1998.
- ²⁴G. M. Sheldrick, SHELXS-97, Program for Crystal Structure Refinement, University of Goettingen, Germany, 1997; Windows version by McArdle, National University of Ireland, Galway.
- ²⁵A. Arrott and J. E. Noakes, *Phys. Rev. Lett.* **19**, 786 (1967).
- ²⁶See, for example, H. Zhang, J. W. Lynn, W.-H. Li, T. W. Clinton, and D. E. Morris, *Phys. Rev. B* **41**, 11229 (1990), where the subtraction technique is discussed and magnetic Bragg cross sections are given.
- ²⁷K. D. Schotte and U. Schotte, *Phys. Lett.* **55A**, 38 (1975).
- ²⁸K. Takegahara, H. Harima, and A. Yanase, *J. Phys. Soc. Jpn.* **70**, 1190 (2001).
- ²⁹E. A. Goremychkin, R. Osborn, E. D. Bauer, M. B. Maple, N. A. Frederick, W. M. Yuhasz, F. M. Woodward, and J. W. Lynn, *Phys. Rev. Lett.* **93**, 157003 (2004).
- ³⁰K. R. Lea, M. J. M. Leask, and W. P. Wolf, *J. Phys. Chem. Solids* **23**, 1381 (1962).
- ³¹A. Ślebarski and D. Wohlleben, *Z. Phys. B: Condens. Matter* **60**, 449 (1985).
- ³²M. B. Maple, Ph.D. thesis, University of California, San Diego, 1969.
- ³³N. A. Frederick and M. B. Maple, *J. Phys.: Condens. Matter* **15**, 4789 (2003).
- ³⁴N. H. Andersen, P. E. Gregers-Hansen, E. Holm, H. Smith, and O. Vogt, *Phys. Rev. Lett.* **32**, 1321 (1974).
- ³⁵P. Rhodes and E. P. Wohlfarth, *Proc. R. Soc. London* **273**, 247 (1963).
- ³⁶T. Moriya, in *Topics in Current Physics 42: Metallic Magnetism*, edited by H. Capellmann (Springer-Verlag, New York, 1987), p.15.
- ³⁷A. Leithe-Jasper, W. Schnelle, H. Rosner, N. Senthilkumaran, A. Rabis, M. Baenitz, A. Gippius, E. Morozova, J. A. Mydosh, and Y. Grin, *Phys. Rev. Lett.* **91**, 037208 (2003).
- ³⁸K. Takegahara and H. Harima, *J. Phys. Soc. Jpn.* **71**, 240 (2002).
- ³⁹A. Mitsuda, T. Goto, K. Yoshimura, W. Zhang, N. Sato, K. Kosuge, and H. Wada, *Phys. Rev. Lett.* **88**, 137204 (2002).
- ⁴⁰P. M. Chaikin and T. C. Lubensky, *Principles of Condensed Matter Physics* (Cambridge University Press, Cambridge, 2000).
- ⁴¹R. V. Chamberlin, *Nature (London)* **48**, 337 (2000).
- ⁴²D. Belitz, T. R. Kirkpatrick, M. T. Mercaldo, and S. L. Sessions,

- Phys. Rev. B **63**, 174427 (2001); **63**, 174428 (2001).
- ⁴³J. J. Binney, N. J. Dowrick, A. J. Fisher, and M. E. J. Newman, *The Theory of Critical Phenomena* (Oxford University Press, New York, 2001).
- ⁴⁴Y. Kats, L. Klein, J. W. Reiner, T. H. Geballe, M. R. Beasley, and A. Kapitulnik, Phys. Rev. B **63**, 054435 (2001).
- ⁴⁵M. Ziese, J. Phys.: Condens. Matter **13**, 2919 (2001).
- ⁴⁶A. Perumal and V. Srinivas, Phys. Rev. B **67**, 094418 (2003).
- ⁴⁷W. M. Yuhasz, N. A. Frederick, P.-C. Ho, N. P. Butch, B. J. Taylor, T. A. Sayles, M. B. Maple, J. B. Betts, A. H. Lacerda, P. Rogl, and G. Giester, Phys. Rev. B **71**, 104402 (2005).
- ⁴⁸E. D. Bauer, A. Ślebarski, N. A. Frederick, W. M. Yuhasz, M. B. Maple, D. Cao, F. Bridges, G. Giester, and P. Rogl, J. Phys.: Condens. Matter **16**, 5095 (2004).